PHYSICAL REVIEW E **92**, 031001(R) (2015)

Viscoelastic Taylor-Couette instability as analog of the magnetorotational instability

Yang Bai, Olivier Crumeyrolle, and Innocent Mutabazi*

Laboratoire Ondes et Milieux Complexes, UMR No. 6294, CNRS, Université du Havre, 53 Rue de Prony, F-76058 Le Havre Cedex, France

(Received 30 May 2015; published 2 September 2015)

A linear stability analysis and an experimental study of a viscoelastic Taylor-Couette flow corotating in the Keplerian ratio allow us to elucidate the analogy between the viscoelastic instability and the magnetorotational instability (MRI). A generalized Rayleigh criterion allows us to determine the potentially unstable zone to pure-elasticity-driven perturbations. Experiments with a viscoelastic polymer solution yield four modes: one pure-elasticity mode and three elastorotational instability (ERI) modes that represent the MRI-analog modes. The destabilization by the polymer viscosity is evidenced for the ERI modes.

DOI: 10.1103/PhysRevE.92.031001 PACS number(s): 47.20.Qr, 47.15.−x, 47.50.Gj, 97.10.Gz

Magnetorotational instability (MRI) is considered as a plausible mechanism that triggers turbulence, responsible for the angular momentum transport in accretion disks [1]. It occurs in differentially rotating fluids of high electric conductivity in the presence of a magnetic field, when the angular velocity decreases with the radial distance [2]. Though the MRI has been well studied theoretically and numerically [1,3], its experimental realization is still technically difficult because large values of the magnetic Reynolds number $\mathrm{Rm} = \dot{\gamma}\tau_\lambda$ and the inertial Reynolds number $\mathrm{Re} = \dot{\gamma}\tau_\nu$ are required [4–6]. Here $\dot{\gamma}$ is the shear rate, $\tau_\lambda = d^2/\lambda$ and $\tau_\nu = d^2/\nu$ represent the magnetic and viscous diffusion times on a characteristic length d, and ν is the kinematic viscosity of the fluid. The magnetic diffusivity is given by $\lambda = 1/\mu\sigma$, where μ and σ are the magnetic permeability and the electric conductivity of the fluid, respectively.

Ogilvie and Proctor [7] have highlighted the similarity between the equations of viscoelastic fluids and those of magnetohydrodynamics (MHD). They found that, among all types of viscoelastic fluids, flows of polymer solutions described by the Oldroyd-B model [8] are governed by equations identical to those of MHD in the limit of infinite polymer relaxation time τ and magnetic diffusion time τ_λ [7]. The Taylor-Couette flow of a viscoelastic fluid between two differentially rotating cylinders represents the flow system where this analogy should be tested. The inner cylinder of radius a rotates at the angular velocity Ω_i and the outer one of radius b rotates at the angular velocity Ω_o. The gap of width $d = b - a$ is filled with a viscoelastic polymer solution of density ρ and viscosity μ_t obtained by dissolving a long-chain polymer in a solvent of viscosity μ_s. The polymer has a relaxation time τ and its contribution to viscosity is defined $\mu_p = \mu_t - \mu_s$. The dimensionless control parameters of the flow are the radius ratio $\eta = a/b$, the rotation ratio Ω_o/Ω_i,the viscosity ratio $S = \mu_p/\mu_t$, the inertial Reynolds number Re, and the Weissenberg number $\mathrm{Wi} = \dot{\gamma}\tau$, where $\dot{\gamma} = (\Omega_i a - \Omega_o b)/d$. The viscous diffusion time is $\tau_\nu = \rho d^2/\mu_t$. The dimensionless flow equations of a polymer solution satisfying the Oldroyd-B model read

$$\nabla \cdot \mathbf{u} = 0,$$

$$\frac{\partial \mathbf{u}}{\partial t} + \mathbf{u}\cdot\nabla\mathbf{u} = -\nabla\psi + \nabla\cdot\mathbf{T} + \frac{1-S}{\mathrm{Re}}\nabla^2\mathbf{u},$$

$$\frac{\partial \mathbf{T}}{\partial t} + \mathbf{u}\cdot\nabla\mathbf{T} - (\nabla\mathbf{u})^t\cdot\mathbf{T} - \mathbf{T}\cdot\nabla\mathbf{u} = -\frac{1}{\mathrm{Wi}}\left\{\mathbf{T} - \frac{S}{\mathrm{Re}}[\nabla\mathbf{u} + (\nabla\mathbf{u})^t]\right\}, \quad (1)$$

where $\mathbf{u}$ and $\mathbf{T}$ represent the velocity field and the polymer stress tensor, respectively, and ψ is the dimensionless generalized pressure.

Ogilvie and Potter [9] have performed a linear stability analysis (LSA) for a viscoelastic fluid described by the Eqs. (1) for three different rotation regimes defined by $\Omega_o/\Omega_i = \eta^q$ with $\eta = 0.95$ and $S = 0.5$; q is the local exponent of the angular velocity [10]. In the Keplerian regime ($q = 3/2$), the instability leads to nonaxisymmetric rotating spiral patterns. The critical value of Re decreases as Wi increases. This instability, which is not driven by the centrifugal force but requires sufficiently large shear and elastic energies, was called the MRI-analog [9] or elastorotational instability (ERI) [11]. The existence of a finite critical value of Wi for $\mathrm{Re} \to 0$ indicates the pure-elasticity-driven instability in the Keplerian regime. For the anti-Keplerian regime ($q = -3/2$), only the pure-elasticity mode is critical, but it is suppressed by the increase of the shear, i.e., of Re. The instability of the flow with $q = 3$ leads to three types of modes: the ERI, the centrifugal instability, and the pure-elasticity instability modes.

We are aware of only one experiment performed to track this analogy, in an aqueous polymer solution of polyethylene oxide (PEO) of 7×10^6 g/mol with relatively large concentrations in a Taylor-Couette system with $\eta = 0.903$ [11]. The nonaxisymmetric spiral mode was observed in solutions with polymer concentrations higher than 0.2% (0.25% and 0.375%) and the axisymmetric vortex mode was found in solutions with a concentration of 0.5%. The corresponding values of S are {0.983,0.991,0.995}. However, no rheological tests of the working fluids were presented to check if the solutions fit the Oldroyd-B model. As only three data points in the plane (Wi,Re) were reported, it is difficult to make a quantitative comparison of these results with those of [9].[1]

*Corresponding author: innocent.mutabazi@univ-lehavre.fr

[1]The Weissenberg number Wi used in the present work is related to the Deborah number De used in [9] as follows: $\mathrm{De} = \mathrm{Wi} - \Omega_o\tau$.

This Rapid Communication aims to confirm the analogy between the viscoelastic instability and the MRI. It gives results of the LSA of the flow of polymer solutions satisfying the Oldroyd-B model and experimental results in a Taylor-Couette system with a radius ratio $\eta = 0.8$ when the cylinders rotate in a Keplerian ratio. A generalized Rayleigh criterion of the stability of a viscoelastic flow is established to identify the potentially unstable zone to pure-elasticity-driven perturbations. The LSA is performed for different values of S. In experiments, different values of S are obtained using many solutions of the same polymer in different solvents. The results from LSA and experiments are compared and confirm the existence of the ERI modes in the viscoelastic Taylor-Couette flow in the Keplerian regime; these modes are the MRI-analog modes.

The analogy between the MRI and the ERI proposed by [7] requires infinite values of Wi, i.e., it works for ideal inviscid MHD and for polymer solution of infinite elasticity. In fact, the modified polymeric stress tensor $\mathbf{T}_p = \mathbf{T} + \mu_p/\tau\mathbf{I}$ and the magnetic stress tensor $\mathbf{T}_M = \mathbf{BB}/\mu_0$ (where $\mathbf{B}$ is the magnetic field) satisfy identical equations in the limit of $\mathrm{Wi} \to \infty$ and $\mathrm{Rm} \to \infty$ [7]. The modified polymeric stress tensor of the viscoelastic circular Couette flow can be represented as [7] ${T_p}^{ij} = {B_{p1}}^i {B_{p1}}^j + {B_{p2}}^i {B_{p2}}^j + {B_{p3}}^i {B_{p3}}^j$, where $\mathbf{B}_{pk}$ ($k = 1,2,3$) is the polymeric analog of the magnetic field. One possible set of vectors $\mathbf{B}_{pk}$ reads

$$\frac{\mathbf{B}_{p_1}}{B_0} = \frac{\sqrt{2}}{2}\begin{pmatrix}1\\0\\0\end{pmatrix}, \quad \frac{\mathbf{B}_{p_2}}{B_0} = \frac{\sqrt{2}}{2}\begin{pmatrix}1\\\frac{C}{r^2}\\0\end{pmatrix}, \quad \frac{\mathbf{B}_{p_3}}{B_0} = \begin{pmatrix}0\\0,\\1\end{pmatrix} \quad (2)$$

where $C = 2\eta^2(1-\mu)\mathrm{Wi}/(1-\eta^2)(1-\eta)(\eta-\mu)$, $B_0 = \hat{E}^{1/2}/\mathrm{Wi}$ is a characteristic polymer-analog of the magnetic field, $E = \mathrm{Wi}/\mathrm{Re}$ is the solution elasticity, and $\hat{E} = ES$ is the polymer contribution to the solution elasticity. Since the radial magnetic field is not active in the destabilization, we compare the azimuthal component of $\mathbf{B}_{p2}$ with the pure axial field $\mathbf{B}_{p3}$. The latter will dominate the dynamics and the ERI will be the analog of the standard MRI (SMRI) if $\mathrm{Wi} \ll \mathrm{Wi}^+$; for $\mathrm{Wi} \gg \mathrm{Wi}^+$ the ERI will be the analog of the azimuthal MRI, where Wi^+ is given by the condition $\sqrt{2}C/2r^2 = 1$. When both components are comparable, one expects that the ERI will appear in the form of helicoidal modes, which should be the analog of helicoidal MRI (HMRI) modes [12].

Equations (1) were linearized about the base flow state and the perturbations were expanded into normal modes of the form $\exp[st + i(kz + m\varphi)]$. Here $s = \sigma + i\omega$, σ and ω are the temporal growth rate and the frequency of the perturbations, k and m are their axial and azimuthal wave numbers, respectively. The resulting equations were solved using the Chebyshev collocation method with the MATLAB eigenvalue solver. We have validated our codes with the Newtonian flow case and then we solved a few cases of available works for viscoelastic flows [9,13,14]. We retrieved the results of [13,14] and our results differ from those of [9] by 10%. We have solved the equations for many values of η, but we present only the results obtained for the case $\eta = 0.8$, which is the radius ratio of our experimental system. We plotted the curves of critical states $\mathrm{Ta}_c(K)$ for different values of S (Fig. 1), where $\mathrm{Ta} = \mathrm{Re}\sqrt{\delta}$ is the Taylor number and $K = \mathrm{Wi}\sqrt{S\delta}$ is the modified

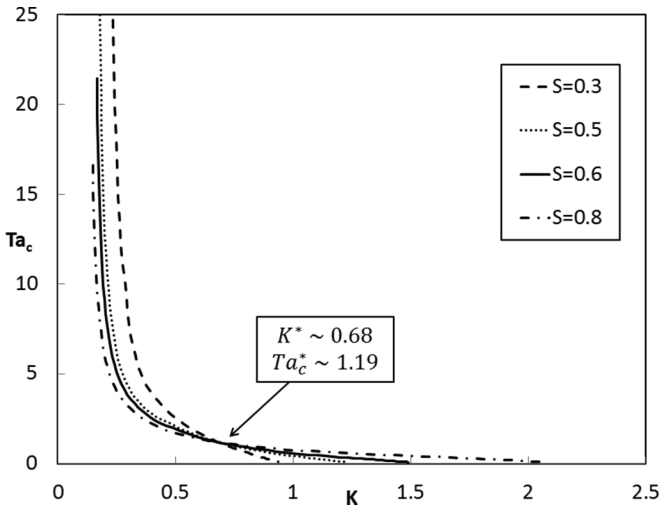

FIG. 1. Curves of critical states for different values of S for $\eta = 0.8$ in the Keplerian regime.

Weissenberg number to take into account the viscosity ratio and the average curvature $\delta = 2(1-\eta)/(1+\eta)$. For each value of S, the curve of critical states has a vertical asymptote $K = K_{\min}(S)$; it does not intersect the vertical axis $K = 0$, in agreement with the stability of the Newtonian flow in the Keplerian regime. On the other hand, this curve intersects the horizontal axis ($\mathrm{Ta} = 0$) at $K_c(\mathrm{Ta} = 0)$, which corresponds to the threshold of the pure-elasticity-driven instability [15–17]. For all values of S, Ta_c decreases when K increases, i.e., the more elastic solution requires a slower rotation shear rate to be destabilized. The critical states have different properties: There is a value K_0 such that for $K_{\min}(S) < K < K_0(S)$ critical modes are axisymmetric and stationary ($m = 0, \omega = 0$), while for $K > K_0(S)$ critical modes are oscillatory nonaxisymmetric with different values of m and ω. The largest value of computed m is $m = 3$ for all values of S. The curves of critical states for different S intersect each other at the point ($K^* \approx 0.68, \mathrm{Ta}_c{}^* \approx 1.19$), which separates each curve $\mathrm{Ta}_c(K)$ into two parts where S plays different roles: For $K < K^*$, larger values of S (i.e., of polymer viscosity) destabilize the flow, while for $K > K^*$, they inhibit the instability. In the vicinity of the cross point, the viscosity ratio S has no influence on the critical parameters. The destabilization by the polymer viscosity is analogous to the dissipation-induced destabilization of the Chandrasekhar solution in MHD [3]. Indeed, the cross point occurs for oscillatory states (waves) and it is possible to define the polymeric analog of the axial Alfvén velocity [18] $v_A = \sqrt{\mu_p/\rho\lambda}$, the dimensionless form of which is $U_A = v_A d\dot{\gamma} = \mathrm{Re}^{-1}\sqrt{S/E} = B_0$. At the cross point ($K^*$,$\mathrm{Ta}_c{}^*$), this polymeric Alfvén velocity is independent of S; it is determined by the elasticity of the solution.

When presented on a map of ($\hat{E}$,Ta), the curves of critical states converge into one curve (Fig. 2). For fluids of small $\hat{E}$, the critical mode appears as an axisymmetric vortex with an axial wavelength smaller than the gap width; when $\hat{E}$ is large, the critical mode is a nonaxisymmetric mode with an axial wave number larger than the gap width. In the small gap limit $\eta \to 1$, the axisymmetric mode is not critical, which is the reason why the study in [9] did not report it for $\eta = 0.95$.

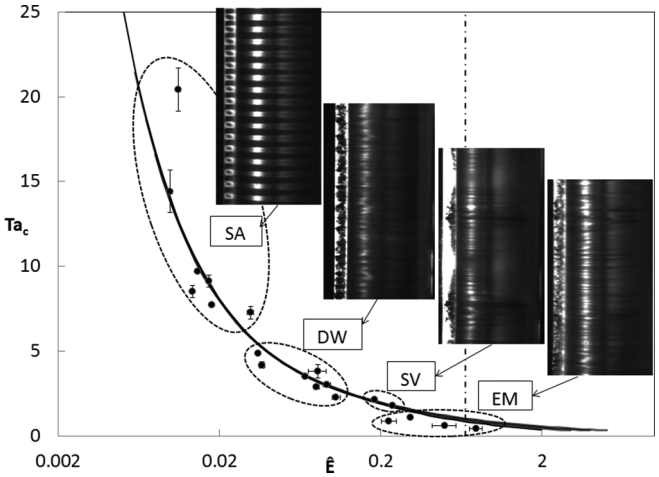

FIG. 2. Stability diagram for $\eta = 0.8$ in the Keplerian regime: solid lines, curves of the critical states predicted by LSA for $S \in 0.5,0.6,0.7,0.8$; closed circles, experimental critical values. The pictures are typical with the cross section of the four modes. Dashed vertical line corresponds to $\hat{E}_0$.

In order to discriminate the pure-elasticity mode from the MRI-analog mode, we derive a stability criterion based on the Rayleigh discriminant (RD) as in the case of the centrifugal instability [2]. Let a fluid particle be suddenly displaced from an orbit r to a new orbit $r + dr$ in such a way that its fly time is very small compared to the viscous diffusion time and to the elastic relaxation time. At the new position, the displaced particle is under the balance between the centrifugal force, the centripetal pressure gradient, and the elasticity force from the first normal stress difference N_1. The dimensionless restoring force acting on the particle is $df = -\Phi(r)dr$, where $\Phi(r) = \Phi_c + \Phi_e$ is the generalized RD. For a Newtonian flow in the Keplerian regime, the centrifugal RD $\Phi_c = (1/r^3)d(rV)^2/dr$ is positive, so the flow is potentially stable [$V(r)$ is the azimuthal velocity of the base flow]. The contribution of the elasticity force is $\Phi_e = (1/r)(dN_1/dr)$. For any viscoelastic flow in curved geometry, the elasticity will amplify the instability if N_1 decreases with the radial distance; otherwise it will inhibit it. For a viscoelastic fluid of the Oldroyd-B model,

$$\Phi_e(r) = -32\hat{E}\left(\frac{1-\mu}{1-\eta^2}\right)^2\left(\frac{\eta}{1-\eta}\right)^4\frac{1}{r^6}. \qquad (3)$$

The generalized RD has the same structure as the one for the Taylor-Couette flow with an azimuthal magnetic field [2,18]. The viscoelastic Taylor-Couette flow is potentially unstable to pure-elasticity-driven perturbations if $\hat{E} > \hat{E}_0$ when the cylinders rotate in the Keplerian ratio and, for $\hat{E} > \hat{E}_1$, if the cylinders rotate in the anti-Keplerian ratio. For $\eta = 0.8$, $\hat{E}_0 = 0.672$ and $\hat{E}_1 = 3.45$. The value $\hat{E} = \hat{E}_0$ is represented by the vertical dashed line (Fig. 2) and separates the plane ($\hat{E}$,Ta) into potentially stable and unstable zones to pure-elasticity-driven perturbations. The point (K^*,Ta*) in Fig. 1 corresponds to $\hat{E} \in [0.32,0.48] < \hat{E}_0$ for $S \in [0.3,0.8]$. So the critical modes observed for $\hat{E} < \hat{E}_0$ can be attributed to the flow destabilization by a combination effect of the elasticity and rotation, which was called ERI. Along the Keplerian line, the flow satisfies the Velikhov-Chandrasekhar stability criterion [2,18] when Wi $\ll$ Wi$^+$. Therefore, these ERI modes are MRI-analog modes.

The experiments were conducted in a Taylor-Couette system with $\eta = 0.8$ and a gap width $d = 1$ cm with the aspect ratio $\Gamma = L/d = 45$, where L is the length of the gap. Both the inner and outer cylinders are thermalized to the temperature of $T = 20\,^\circ\text{C} \pm 0.4\,^\circ\text{C}$. The cylinders are driven by two motors in such a way that their angular velocities are in the ratio η^q. The working solutions consist of 1000 parts per 10^6 (by weight) of high molecular PEO molecules (8×10^6 g/mol) dissolved in a solvent made by water, 2.5% of isopropyl alcohol and polyethylene glycol (PEG) (2×10^4 g/mol), the concentration of which varies from 2.5% to 25% by weight. For visualization, 2% of aqueous Kalliroscope suspension was added into the solutions. In such a weak concentration, it does not modify the solution viscosity [19]. The PEO and the PEG have the same chemical structure H—(O—CH$_2$—CH$_2$)$_n$—OH; they differ by the degree of polymerization n. In our experiment, $n_{\text{PEG}} \simeq 450$ and $n_{\text{PEO}} \simeq 1.8 \times 10^5$. The PEO works as a source of both the elasticity and viscosity while the PEG increases only the solution viscosity. The viscosity of the solvent μ_s and that of the solution μ_t were measured with a shear rheometer (MCR 501). The solvent viscosity was constant for all shear rates. The total viscosity μ_t of solutions is constant except for solutions with low PEG concentrations where it shows a weak shear thinning over two decades of shear rates. So we assumed that the solutions could be described approximately by the Oldroyd-B constitutive equation as the shear rates in the experiment cover only one decade. The relaxation time was measured from the first normal stress difference (τ_{N_1}) and by the extensional rheometer CaBER (τ_e). For each solution, μ_t and τ_e were measured before and after the experiment in the Taylor-Couette system to verify if the polymers have experienced any damage, e.g., if there is any decrease of viscosity and the relaxation time. The molecular relaxation time was estimated from μ_p as $\tau_M = \mu_p/cRT$, where c is the polymer concentration and R is the universal gas constant. The relaxation times of the working solutions vary from 0.06 to 0.5 s, so their elasticity E varies from 0.01 to 1.5 and the viscosity ratio S varies from 0.45 to 0.87. For all solutions, $\tau_{N_1} < \tau_M < \tau_e$ and we used τ_M to compute the experimental values of Wi, K, and E. For each solution, i.e., for each value of $\hat{E}$, the angular velocity of both cylinders was increased step by step, with a waiting period of 20 min until the vortex patterns appeared in the flow. The cross section of the flow patterns was visualized with a vertical laser sheet (pictures in Fig. 2). The critical values of the angular velocity at which the patterns were formed in the flow were recorded. The critical points are represented in the stability diagram ($\hat{E}$,Ta$_c$) (Fig. 2). The experimental data show a net destabilization of the viscoelastic circular Couette flow in the Keplerian regime. Weak elastic solutions require large values of shear rate to be destabilized, while high elastic solutions require a weak shear rate to be destabilized in the presence of curvature.

Four different modes (gathered by ellipses in Fig. 2) were observed in the experiment. For small values of $\hat{E}$, the critical mode is a stationary axisymmetric (SA) mode composed of vortices with an axial wavelength smaller than the gap width [i.e., vortices that are flattened in the gap (Fig. 2)]. For

intermediate values of $\hat{E}$, the critical mode is a disordered wave (DW) mode or a solitary vortex (SV) mode. The DW mode results from the superposition of spiral vortices that are created near the top and bottom endplates and propagate towards the center of the system. For all runs, spiral vortices are transient, they interact nonlinearly to give rise to waves disordered in space but periodic in time. Their averaged axial wavelength is about 1.40 ($\pm$0.04) as predicted by LSA. The SV mode is composed of irregular in space and time intense localized vortices separated by large zones occupied by disordered waves; they are strongly nonlinear as a result of coupling of traveling waves of different wavelengths. Similar structures have been reported in [20]. For large values of $\hat{E}$, the critical mode is a pure-elasticity mode (EM). This mode appears in the form of a chaotic pattern of irregular vortices [15,21]. It is located on the right side of the critical value of $\hat{E}_0$ and thus it is the result of the flow destabilization by the elasticity force as predicted by the generalized RD. It requires streamline curvature and a small shear to be triggered. When the cylinders are rotating in an anti-Keplerian ratio, the same EM was observed at $4\,\mathrm{Ta}_c$. The transition from the circular Couette flow to the SA mode is supercritical; no hysteresis was found when ramping up and down. The transitions to the three other modes present a significant hysteresis and are therefore subcritical. The SA, DW, and SV modes were not observed in the anti-Keplerian regime, hence they are the ERI modes that represent the MRI-analog modes. The elasticity mode is observed in the anti-Keplerian regime and therefore it is related to the pure-elasticity-driven instability; it is not the analog the MRI. The fact that the three MRI-analog modes are observed for $\hat{E} < \hat{E}_0$ highlights the importance of the polymer viscosity in the flow destabilization of the Keplerian regime.

According to [7], the strict analogy works between non-viscous ideal magnetic fluids and viscoelastic fluids with infinite relaxation time. These conditions are not satisfied in the experiment. The experimental results are in good agreement with LSA results: Both axisymmetric modes and nonaxisymmetric modes were observed (although the latter were observed in a nonlinear regime). The tendency of the threshold to decrease with the elasticity is recovered. The discrepancy observed for small values of $\hat{E}$ is related to the weak shear-thinning behavior of the working solutions. For large values of $\hat{E}$, the solutions fit better the Oldroyd-B model. The SA modes were obtained for low values of $\hat{E}$, for which the axial polymeric-analog field $\mathbf{B}_{p3}$ dominates the field $\mathbf{B}_{p2}$. This mode is therefore the analog of the SMRI. The DW and the SV modes were obtained for values of $\hat{E}$ for which the axial field $\mathbf{B}_{p3}$ has the same order of magnitude as the azimuthal component of $\mathbf{B}_{p2}$. The DW mode is a nonlinear superposition of two counterpropagating spirals, hence it is the analog of the HMRI. The results of [11] reported helicoidal modes in the same range of E as in our case, but the axisymmetric mode was observed for large values of E for which LSA predicts SA modes. This difference may be related to the difference in values of η and S. The SV mode is a different mode; its analogy with MRI should be investigated in more detail.

The present study of the viscoelastic Taylor-Couette flow in the Keplerian regime confirms the analogy conjectured by Ogilvie and Proctor [7] between ERI and MRI. Among different critical modes, SA, DW, and SV modes are due to ERI and are good candidates for the MRI-analog modes.

We thank Ch. Egbers, N. Herzog, and O. Kirillov for fruitful discussions about this project. This work has benefited from support from the CPER and the French National Research Agency (ANR), through the program Investissements d'Avenir (Grant No. ANR-10 LABX-09-01), LABEX EMC^3. Y.B. has benefited from a doctoral grant from the University of Le Havre.

[1] S. A. Balbus and J. F. Hawley, Rev. Mod. Phys. **70**, 1 (1998).
[2] S. Chandrasekhar, *Hydrodynamic and Hydromagnetic Stability* (Oxford University Press, Oxford, 1961).
[3] O. N. Kirillov, F. Stefani, and Y. Fukumoto, J. Fluid Mech. **760**, 591 (2014).
[4] R. Hollerbach and G. Rudiger, Phys. Rev. Lett. **95**, 124501 (2005).
[5] H. Ji, M. Burin, E. Schartman, and J. Goodman, Nature (London) **444**, 343 (2006).
[6] E. Schartman, H. Ji, M. J. Burin, and J. Goodman, Astron. Astrophys. **543**, A94 (2012).
[7] G. I. Ogilvie and M. R. E. Proctor, J. Fluid Mech. **476**, 389 (2003).
[8] R. B. Bird, R. C. Armstrong, O. Hassager, and C. F. Curtiss, *Dynamics of Polymeric Liquids* (Wiley, New York, 1977).
[9] G. I. Ogilvie and A. T. Potter, Phys. Rev. Lett. **100**, 074503 (2008).
[10] B. Dubrulle, O. Dauchot, F. Daviaud, P.-Y. Longaretti, D. Richard, and J.-P. Zahn, Phys. Fluids **17**, 095103 (2005).
[11] S. Boldyrev, D. Huynh, and V. Pariev, Phys. Rev. E **80**, 066310 (2009).
[12] F. Stefani, T. Gundrum, G. Gerbeth, G. Rudiger, M. Schultz, J. Szklarski, and R. Hollerbach, Phys. Rev. Lett. **97**, 184502 (2006).
[13] M. Avgousti and A. N. Beris, J. Non-Newt. Fluid Mech. **50**, 225 (1993).
[14] E. Kupferman, J. Comput. Phys. **147**, 22 (1998).
[15] R. Larson, E. S. G. Shaqfeh, and S. J. Muller, J. Fluid Mech. **218**, 573 (1990).
[16] E. S. G. Shaqfeh, Annu. Rev. Fluid. Mech. **28**, 129 (1996).
[17] A. Groisman and V. Steinberg, Phys. Fluids **10**, 2451 (1998).
[18] P. A. Davidson, *Turbulence in Rotating Stratified and Electrically Conducting Fluids* (Cambridge University Press, Cambridge, 2013).
[19] O. Crumeyrolle, I. Mutabazi, and M. Grisel, Phys. Fluids **14**, 1681 (2002).
[20] B. M. Baumert and S. J. Muller, J. Non-Newt. Fluid Mech. **83**, 33 (1999).
[21] A. Groisman and V. Steinberg, Phys. Rev. Lett. **78**, 1460 (1997).